Nuclear Shell Structure at Particle Drip Lines

J. Dobaczewski,* I. Hamamoto,† W. Nazarewicz,* and J. A. Sheikh‡
Joint Institute for Heavy-Ion Research, Physics Division, Oak Ridge National Laboratory, P.O. Box 2008, Oak Ridge, Tennessee 37831
and Department of Physics, University of Tennessee, Knoxville, Tennessee 37996
(Received 1 September 1993)

The shell structure of exotic nuclei near proton and neutron drip lines is discussed in terms of the self-consistent mean-field theory. It is demonstrated that when approaching the neutron drip line, the neutron density becomes very diffused and the single-particle spectrum shows similarities to that of the harmonic oscillator with spin-orbit term. Interaction between bound orbitals and continuum is shown to result in quenching of shell effects in light and medium systems.

PACS numbers: 21.10.Dr, 21.10.Ft, 21.10.Pc, 21.60.Jz

Nuclei far from stability have never been as close to us as they are now—thanks to exotic (radioactive) ion beam facilities currently under construction in Europe, the U.S.A., and Japan. Partly due to those experimental developments the physics of exotic nuclei is one of the fastest developing subjects in nuclear physics. In the medium mass and heavy nuclei, explorers are going beyond the proton drip line and approaching very neutron-rich systems [1,2].

In contrast to the nuclear shell structure along the beta-stability line which has been well studied both experimentally and theoretically, the yet unknown shell structure in drip-line nuclei is currently of great interest. Theoretically, radioactive ion beam physics is a challenge for well established models of nuclear structure and, because of the dramatic extrapolations involved, it invites a variety of theoretical approaches. Since the parameters of interactions used in the usual mean-field calculations, such as the Skyrme interaction in the Hartree-Fock (HF) approach, are determined so as to reproduce the properties of beta-stable nuclei, the parameters may not always be proper to be used in the calculation of drip-line nuclei. In fact, the predicted drip lines strongly depend on the models employed [3–7].

In this Letter, the global properties of the shell structure of drip-line nuclei are discussed by means of three state-of-the-art mean-field models, namely the HF and the Hartree-Fock-Bogoliubov (HFB) models with Skyrme-type interactions, and the relativistic mean-field approximation (RMF). Limiting ourselves to the calculations of spherical shape we examine the quantities which show striking differences between the shell structure of beta-stable nuclei and drip-line nuclei.

Using the SkP variant of Skyrme interaction [8], which was obtained by fitting global properties of several magic nuclei together with the tin isotopes, we solve the HF or HFB equations in the coordinate space [8] with the box radius of 20 fm. The basic ingredients in the RMF approach [9] are the baryons and the mesons. In the present version of the RMF approach the NL1 force [10] was employed. The resulting equations of motion are solved by means of the basis expansion method. The number of spherical oscillator shells used in the present work is 20 for both the Dirac spinors and for the meson fields. The details of this basis expansion method can be found in Ref. [11].

The average spherical nuclear potential (optical potential) is usually approximated by a field

$$U(r) = V_0 f(r) + V_{ls} \frac{1}{r} \frac{d}{dr} f(r)(\boldsymbol{l} \cdot \boldsymbol{s}), \tag{1}$$

where

$$f(r) = \left[1 + \exp\left(\frac{r - r_0 A^{1/3}}{a}\right)\right]^{-1} \tag{2}$$

is the Woods-Saxon–type radial form factor and the central and spin-orbit potential depths, V_0 and V_{ls}, weakly depend on the neutron excess through the isovector term, proportional to $I = (N-Z)/A$. The single-particle states of (1) in beta-stable nuclei exhibit the characteristic gradual dependence on mass number A, namely, the increased nuclear radius leads to a systematic increase in the orbital binding energy (cf. Figs. 2–30 shown in Ref. [12]). In order to analyze the trends towards drip-line nuclei, we investigate the *isobaric chains* of nuclei with a constant A.

The extreme situation expected at the $A = 100$ drip lines is displayed in Fig. 1 for the proton-drip-line nucleus $^{100}_{50}\mathrm{Sn}_{50}$ and the neutron-drip-line nucleus $^{100}_{30}\mathrm{Zn}_{70}$. Here we show the self-consistent proton and neutron densities, and the central potentials (plus the Coulomb potential for protons). It is seen that the densities calculated in the HF and RMF models are indeed fairly similar. We have also checked that the results obtained from the HF calculations using the SIII [13] or the SkM* interaction [14], and the RMF results with the NL-SH interaction [15], are very similar to those shown in Fig. 1. A striking feature seen in the neutron-drip-line nucleus ^{100}Zn is the presence of a pronounced diffuseness in the neutron density as well as in the proton potential. It is clearly seen that the proton (neutron) potential is more strongly affected by the neutron (proton) density than by the proton (neutron) density [16]. The 30 protons in ^{100}Zn occupy the deeply bound levels. Consequently, the resulting dif-

0031-9007/94/72(7)/981(4)$06.00

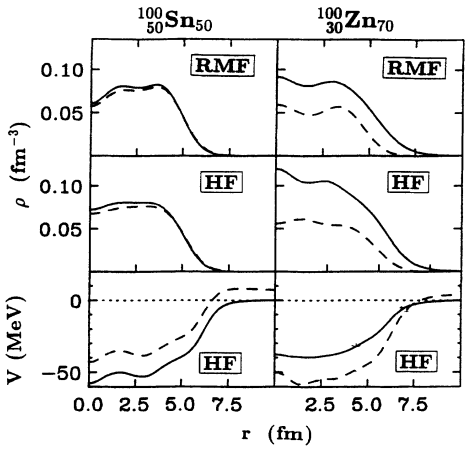

FIG. 1. Top: Single-particle nucleonic densities of the NL1 RMF model for the $A = 100$ drip-line nuclei, ^{100}Sn and ^{100}Zn (neutrons: solid line, protons: dashed line). Middle (bottom): corresponding single-particle densities (central potentials) of the SkP HF approach.

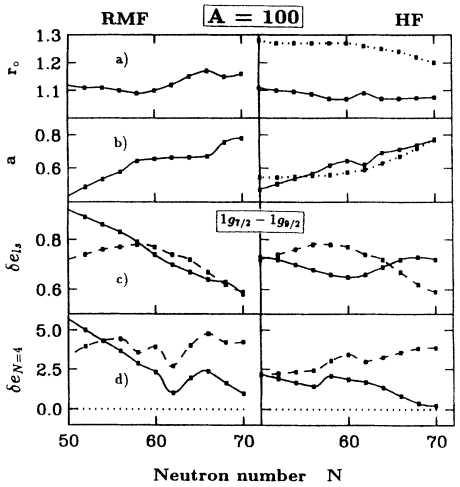

FIG. 2. (a) Effective radius r_0 [in fm; cf. Eq. (2)] of the single-particle neutron density of the RMF (left) and HF (right) model as a function of N for $A = 100$ isobars. For comparison, the effective radius of the central HF neutron potential is denoted by the dotted line. (b) Effective diffuseness a (in fm). (c) The spin-orbit splitting δe_{ls} (in MeV) given by Eq. (6) for the $1g$ shell (neutrons: solid line, protons: dashed line). Note systematic differences between RMF and HF results. (d) The effective N=4 shell splitting, $\delta e_{N=4}$=$\delta e_{ll}(3s)$–$\delta e_{ll}(1g)$, [in MeV; see Eq. (7)]. It is worth noting that the neutron shell splitting approaches zero at the neutron-drip line.

fuseness of the proton density is not large.

The effective diffuseness $a^{(\rho)}$ and the radius parameter $r_0^{(\rho)}$ of the calculated neutron densities of $A = 100$ nuclei as a function of the neutron number are presented in Fig. 2 [parts (a) and (b)]. They were obtained by comparing the radial moments, $\langle r \rangle$ and $\langle r^2 \rangle$, computed for self-consistent densities with the radial moments resulting from the Fermi distribution (2) [17]. From Fig. 2(b) it is seen that for a given mass number ($A = 100$) the effective HF and RMF diffusenesses of neutron densities are very similar; they increase dramatically when approaching the neutron-drip-line nuclei. The neutron radius parameter, $r_0^{(\rho)}$, shows weak variations with N. For comparison, the values of $a^{(V)}$ and $r_0^{(V)}$ for the central HF neutron potential are also displayed in Figs. 2(a) and 2(b). It is seen that while $a^{(V)} \approx a^{(\rho)}$, the values of $r_0^{(V)}$ are systematically larger than $r_0^{(\rho)}$. The results presented in Fig. 2(b) indicate that the average Woods-Saxon–type potentials used in the Nilsson-Strutinsky calculations for nuclei far from stability should contain an explicit isospin dependence of $a^{(V)}$. It is also interesting to note that for the systems with large diffuseness the energy of the finite-range liquid-drop model [18] becomes rather insensitive to higher-order multipole distortions. This means that the higher-order deformations of such systems are solely determined by the shell effects.

In the upper part of Fig. 3 the HF single-particle energies for the $A = 120$ isobars are plotted as a function of N. Because of the finite radius of the box the calculated single-particle levels with positive energies (continuum) are discrete. The results obtained in the RMF model are very similar (the positive-energy discrete states in RMF appear here as a result of the truncated oscillator basis). Both in the HF and RMF calculations it is seen that the bulk single-particle shell structure exhibited by bunching of *bound* levels and the presence of magic gaps at particle numbers 28, 50, and 82 does not appreciably change as one approaches the neutron-drip line. However, the close inspection of single-particle diagrams in Fig. 3 shows that there are systematic changes in the fine details of shell structure; see below.

The positive-energy low-j continuum manifests itself through the presence of many levels which practically do not vary as a function of N. Indeed, since those states are not localized inside the nuclear volume their dependence on the details of average potential is expected to be very weak (a weak Z dependence of proton continuum results from the change in Coulomb potential). It is also seen that the combined effect of centrifugal and Coulomb forces gives rise to positive-energy states which try to preserve their shell structure. Those can be interpreted as quasibound resonances, especially pronounced for protons (as seen in Fig. 1 the Coulomb barrier varies from ~5 MeV in ^{100}Zn to ~9 MeV in ^{100}Sn).

The pairing force may have a unique role in drip-line nuclei due to the scattering of nucleonic pairs from bound states to positive-energy orbitals. In the HF model with the state-independent seniority pairing (HF+BCS) this leads to the presence of an unphysical "particle gas" surrounding the nucleus [8]. Indeed, the seniority pairing interaction does not introduce any selection rule for initial and final states of a pair; it indiscriminately scatters pairs of particles from bound states to *all* positive-energy states. This problem is overcome in the HFB method

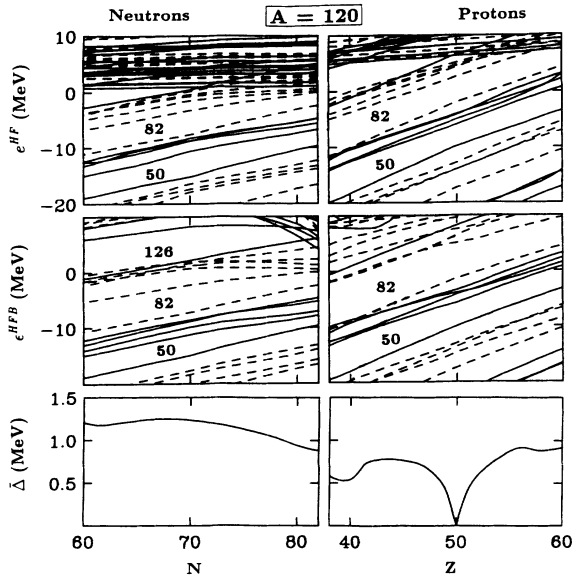

FIG. 3. Spherical single-particle levels for the A=120 isobars calculated in the SkP HF model (top) and SkP HFB model (middle) as a function of neutron number. The single-particle canonical HFB energies are given by $\epsilon_k=\langle\Psi_k|h|\Psi_k\rangle$. Solid (dashed) lines represent the orbitals with positive (negative) parity. The bottom portion shows the average neutron and proton gaps defined by $\bar{\Delta} = \int \Delta(\boldsymbol{r})\rho(\boldsymbol{r})d^3r / \int \rho(\boldsymbol{r})d^3r$.

with a realistic pairing interaction in which the coupling of bound states to continuum is correctly taken into account [8]. (The importance of pairing interaction near drip lines was discussed, e.g., in Ref. [19].)

In order to describe the coupling between bound states and continuum due to pairing we performed the HFB calculations with the SkP force in both particle-hole and particle-particle channels. In the HFB method the underlying shell structure does not have a straightforward interpretation in terms of the eigenvalues of the HFB Hamiltonian, i.e., quasiparticle energies E_α. In order to learn about underlying shell effects one can consider the basis of canonical states which diagonalize the single-particle density matrix

$$\rho(\boldsymbol{r},\boldsymbol{r}') = \sum_k n_k \Psi_k(\boldsymbol{r})\Psi_k^*(\boldsymbol{r}'), \tag{3}$$

where n_k's are the single-particle occupation numbers. Since ρ goes to zero at large distances, the canonical states with $n_k>0$ are always well localized. This is in contrast to the HF states belonging to the positive-energy spectrum. The lower portion of Fig. 3 shows the expectation values $\epsilon_k=\langle\Psi_k|h|\Psi_k\rangle$ of the single-particle Hamiltonian, $h=\delta E_{\rm HFB}/\delta\rho$ [20], in the canonical basis. It is interesting to notice that the single-particle part of the HFB shell-correction energy can be written as

$$\Delta E^{\rm s.p.}_{\rm HFB} = \sum_k n_k\epsilon_k - \left\langle \sum_k n_k\epsilon_k \right\rangle, \tag{4}$$

where $\langle\ \rangle$ means Strutinski-type averaging [20]. Equation (4) suggests that the single-particle canonical energies ϵ_k carry most information on the shell energy. Additional argument for associating ϵ_k with shell structure comes from the analysis of quasiparticle energies E_α. It is well known [20] that if the pair-gap matrix, $\Delta_{k\bar{k}'}$, is diagonal in the canonical basis of a self-consistent solution, the coupling $\langle\Psi_k|h|\Psi_{k'}\rangle$ $(k\neq k')$ disappears and the quasiparticle energy is simply given by

$$E_k = \sqrt{(\epsilon_k-\lambda)^2+\Delta^2_{k\bar{k}}}, \tag{5}$$

where λ is the chemical potential. For realistic interactions the pair-gap matrix is not diagonal. However, since pairing forces are short ranged, one can expect the off-diagonal matrix elements of $\Delta_{k\bar{k}'}$ to be significantly smaller than the diagonal ones. Indeed, according to our calculations the average neutron-number dependencies of low-lying quasiparticle energies obtained from HFB and from Eq. (5) are similar. Consequently, the low-lying quasiparticle excitations and proton and neutron separation energies, $S\simeq\lambda+E_k$, are governed by ϵ_k's. However, only the states in the vicinity of λ have a clear interpretation in the self-consistent theory and values of ϵ_k far from λ are less relevant.

For the isobaric chain of $A = 120$, the neutron Fermi energy approaches zero near $N = 82$. As seen in Fig. 3, the $N = 82$ shell gap dramatically decreases near the neutron-drip line. This effect is primarily caused by a lowering of single-particle (canonical) energies of low-j orbitals relative to those of high-j orbitals. Such an effect results from a strong interaction between bound orbitals and low-j continuum, whereas the interaction with high-j resonance states is much less effective in modifying bound orbitals. For heavier systems with $N > 82$ there are more high-j orbitals in major shells and the lowering of low-j subshells (which, in addition, are located at the top of shells) is not sufficient to close the gaps. Therefore, the quenching of shell effects at the neutron-drip line is only expected in the systems with $N \leq 82$. At the proton-drip line, the quenching occurs only for light systems with $Z \leq 28$, because the Coulomb barrier prevents low-j continuum from approaching bound states. A quenching of this type has recent been demonstrated by the SkP HFB calculations of spherical drip lines [7].

In part (c) of Fig. 2 the spin-orbit splittings of one-particle HF levels,

$$\delta e_{ls} \equiv \frac{1}{2l+1}\left(e_{nl,j=l-1/2} - e_{nl,j=l+1/2}\right), \tag{6}$$

are plotted for $1g$ orbitals in $A = 100$ nuclei as a function of neutron number. For the neutrons, there is no clear dependence of δe_{ls} on N in the HF model. Interestingly, the RMF approach gives the neutron spin-orbit splitting that gradually decreases with N. This result is at variance with the conclusion of Ref. [5]; i.e., the isovector contribution to the spin-orbit potential is not negligible. The proton spin-orbit splitting is fairly simi-

lar in both models; it changes significantly with N and there is a tendency to reduce $(\delta e_{ls})_p$ when approaching the neutron-drip line.

Figure 2(d) displays the calculated N=4 shell splitting for A=100 isobars. It is defined as $\delta e_{N=4} \equiv \delta e_{ll}(3s) - \delta e_{ll}(1g)$, where $\delta e_{ll}(nl)$ are single-particle energies averaged over respective spin-orbit partners, i.e.,

$$\delta e_{ll}(nl) \equiv \frac{l}{2l+1} e_{nl,j=l+1/2} + \frac{l+1}{2l+1} e_{nl,j=l-1/2}. \quad (7)$$

It is seen that the neutron $\delta e_{N=4}$ decreases towards the neutron-drip line. This effect results from the fact that the diffuseness of the one-body neutron potential becomes larger as neutron numbers increase. Consequently, the shape of the potential becomes more similar to that of an oscillator potential (see Fig. 1) and the neutron single-particle spectrum for systems with large neutron excess can be well approximated by that of the Nilsson model without the l^2 term. This observation also suggests that the concept of pseudospin [21–23], based on the delicate balance between the $\boldsymbol{l} \cdot \boldsymbol{s}$ and l^2 terms in the one-body Hamiltonian, should break down at large values of N.

Recently, a new force in the RMF theory has been proposed [15]. We checked that this NL-SH interaction produces results which agree qualitatively with the results of the NL1 RMF calculations presented in this Letter.

In conclusion, our self-consistent HF and RMF analysis indicates that there is a significant isospin dependence of spherical shell effects in medium-mass and heavy nuclei. It is found that (a) the shell structure of neutron-drip-line nuclei is dramatically affected by the interaction with continuum, (b) there are significant differences between predictions of HF and RMF models for isospin dependence of the neutron spin-orbit splitting, and (c) due to large diffusenesses of neutron density and central potential the single-particle spectrum of neutron-drip-line nuclei resembles that of the harmonic oscillator with the spin-orbit term.

Oak Ridge National Laboratory is managed for the U.S. Department of Energy by Martin Marietta Energy Systems, Inc. under Contract No. DE-AC05-84-OR21400. The Joint Institute for Heavy Ion Research has as member institutions the University of Tennessee, Vanderbilt University, and the Oak Ridge National Laboratory; it is supported by the members and by the Department of Energy through Contract No. DE-FG05-87ER40361 with the University of Tennessee. Theoretical nuclear physics research at the University of Tennessee is supported by the U.S. Department of Energy through Contract No. DE-FG05-93ER40770. This research was supported in part by the Polish Committee for Scientific Research under Contract No. 20450 91 01.

* Permanent address: Institute of Theoretical Physics, Warsaw University, Hoża 69, 00-681 Warsaw, Poland.
† Permanent address: Department of Mathematical Physics, Lund Institute of Technology, Box 118, S-22100 Lund, Sweden.
‡ Permanent address: Tata Institute of Fundamental Research, Colaba, Bombay-400 005, India.

[1] *Physics and Techniques of Secondary Nuclear Beams*, edited by J.F. Bruandet, B. Fernandez, and M. Bex (Editions Frontières, Gif-sur-Yvette, 1992).
[2] E. Roeckl, Rep. Prog. Phys. **55**, 1661 (1992).
[3] M. Beiner, R.J. Lombard, and D. Mas, Nucl. Phys. **A249**, 1 (1975).
[4] P. Möller *et al.*, At. Data Nucl. Data Tables **39**, 225 (1988).
[5] D. Hirata *et al.*, Phys. Rev. C **44**, 1467 (1991).
[6] Y. Aboussir *et al.*, Nucl. Phys. **A549**, 155 (1992).
[7] R. Smolańczuk and J. Dobaczewski, Phys. Rev. C **48**, 2166 (1993).
[8] J. Dobaczewski, H. Flocard, and J. Treiner, Nucl. Phys. **A422**, 103 (1984).
[9] B.D. Serot and J.D. Walecka, Adv. Nucl. Phys. **198**, 1 (1986).
[10] P.G. Reinhard *et al.*, Z. Phys. A **323**, 13 (1986).
[11] J.A. Sheikh and P. Ring, Phys. Rev. C **47**, R1850 (1993), and references therein.
[12] A. Bohr and B.R. Mottelson, *Nuclear Structure* (Benjamin, New York, 1969), Vol. 1.
[13] M. Beiner *et al.*, Nucl. Phys. **A238**, 29 (1975).
[14] J. Bartel *et al.*, Nucl. Phys. **A386**, 79 (1982).
[15] M.M. Sharma, M.A. Nagarajan, and P. Ring, Phys. Lett. B **312**, 377 (1993).
[16] D. Vautherin and D.M. Brink, Phys. Rev. C **5**, 626 (1972).
[17] L.R. Elton, *Nuclear Sizes* (Oxford University Press, Oxford, 1961), Appendix C.
[18] H.J. Krappe, J.R. Nix, and A.J. Sierk, Phys. Rev. C **20**, 992 (1979).
[19] G.F. Bertsch and H. Esbensen, Ann. Phys. (N.Y.) **209**, 327 (1991).
[20] P. Ring and P. Schuck, *The Nuclear Many-Body Problem* (Springer-Verlag, Berlin, 1980).
[21] K.T. Hecht and A. Adler, Nucl. Phys. **A137**, 129 (1969).
[22] A. Arima, M. Harvey, and K. Shimizu, Phys. Lett. **30B**, 517 (1969).
[23] C. Bahri, J.P. Draayer, and S.A. Moszkowski, Phys. Rev. Lett. **68**, 2133 (1992).